Asian Journal of Electrical Sciences
ISSN: 2249-6297 (P) Vol.5 No.1, 2016, pp.13-25

DOI: https://doi.org/10.51983/ajes-2016.5.1.1969

Analysis of Elastic Flexural Waves in Non-Uniform Beams Based on Measurement of Strains and Accelerations

Mohammad Amin Rashidifar[1], Ali Amin Rashidifar[2] and Abdolah Abertavi[3]
[1]Department of Mechanical Engineering, Islamic Azad University, Shadegan Branch, Shadegan, Iran
[2]Department of Computer Science, Islamic Azad University, Shadegan Branch, Shadegan, Iran
[3]Department of Electrical Engineering, Islamic Azad University, Shadegan Branch, Shadegan, Iran
Corresponding author E-mail: rashidifar_58@yahoo.com
(Received 23 December 2015; Revised 19 January 2016; Accepted 6 February 2016; Available online 14 February 2016)

Abstract **- Elastic flexural waves in an unloaded and unsupported segment of a non-uniform beam were considered. A method based on Timoshenko's model was established for evaluation of shear force, transverse velocity, bending moment and angular velocity at an arbitrary section from four independent measurements of such quantities at one to four sections. From the evaluated quantities, shear stress, power transmission, etc. can be obtained. Experimental tests were carried out with an aluminium beam which had an abrupt change in height from 15 to 20 mm and was equipped with strain gauges and accelerometers at four uniformly distributed measurement sections and at three evaluation sections. The distance between the two outermost measurement sections was 600 mm, corresponding to 1.12 wave lengths at the upper end of the frequency interval 2500 Hz considered. Bending moments and transverse velocities evaluated from four measurements of any one of these quantities agreed well with those measured at evaluation sections located (i) centrally among the measurement sections and (ii) at a distance of 100 mm, or 0.17 wave lengths, outside. When it was located (iii) at a distance of 500 mm, or 0.83 wave lengths, outside, there was relatively large disagreement as expected from error analysis.**
Keywords: **Elastic Flexural Wave, Unloaded Segment, Uniform Beam, Timoshenko Theory.**

I. INTRODUCTION

Generation of elastic flexural waves in beams occurs in different technological processes, often as a side effect. In percussive drilling of rock, e.g., use is made of elastic extensional waves, but due to eccentric impacts, drill rods that are not perfectly straight [1], unsymmetrical loading of the drill bit [2], etc., flexural waves are also generated. This gives rise to, e.g., leakage of energy from the extensional waves, increased stress levels and increased generation of noise. If the predominant wavelengths are at least of the order of the transverse dimensions of the beam, the motion of flexural waves can be examined by using the Timoshenko beam model. If they are much longer, the wave motion can be studied also by using the Euler-Bernoulli beam model [3].

In various applications, and for different purposes, it is interesting to know the histories of shear force, transverse velocity, bending moment and angular velocity associated with flexural waves at one or several sections of a beam. From them, histories of other important quantities such as shear stress, deflection, normal stress, rotation of a cross-section and power transmission can also be determined.

For elastic extensional waves, Lundberg and Henchoz [4] showed that histories of normal force and particle velocity at an arbitrary section E of a uniform bar can be evaluated from measured strains at two different sections A and B by solving time-domain difference equations which are exact in relation to the one-dimensional theory used. A similar method was used by Yanagihara [5] to determine impact force. Lagerkvist and Lundberg [6], Lagerkvist and Sundin [7] and Sundin [8] used the method to determine mechanical point impedance. The method was used also by Karlsson *et al*. [9] in a study of the interaction of rock and bit in percussive drilling. It was extended to non-uniform bars by Lundberg *et al*. [10], and this version of the method was used for determination of force-displacement relationships for different combinations of drill bits and rocks by Carlsson *et al*. [11] and for high-temperature fracture mechanics testing by Bacon *et al*. [12, 13]. The use of the method was extended to visco-elastic extensional waves by Bacon [14, 15].

The aim of the present paper is to develop a method for evaluation of the histories of shear force, transverse velocity, bending moment and angular velocity at an arbitrary section E of a non-uniform beam from measurements of such quantities at different sections A, B, C and D. It will be shown that, for an unloaded segment of the beam, this can be achieved through measurement of altogether four such quantities which differ from each other in terms of either section (A, B, C and D) or type of quantity (shear force, transverse velocity, bending moment and angular velocity), or both.

First, the method will be developed on the basis of Timoshenko's beam model. Then, experimental impact tests with a non-uniform beam made of aluminium and equipped with strain gauges and accelerometers will be presented, and comparisons will be made between (i) bending moments and particle velocities evaluated at section E on the basis of measurements at sections A-D and (ii) the same quantities measured at section E.

II. THEORETICAL BASIS

A.FORMULATION OF THE PROBLEM

Consider a segment of a non-uniform Timoshenko beam with cross-sectional area $A(x)$, moment of inertia $I(x)$, Young's modulus $E(x)$, shear modulus $G(x)$ and density $\rho(x)$, where x is a co-ordinate along the straight centre line of the beam. For a rectangular cross-section, as in the experimental part, $A = WH$ and $I = WH^3/12$, where W is the width and H is the height. The shear modulus is related to the Young's modulus by the relation $G = E/2(1+\nu)$, where ν is Poisson's ratio. Within the beam segment, there must be no loads, supports, joints or spots of contact. Outside, where there are no such restrictions, the beam is assumed to interact with supports, structures and loads. The supports and structures may have linear or non-linear responses, and they are assumed to have the capability to absorb energy associated with vibrations. Furthermore, the loads are assumed to act during finite time. Otherwise, nothing needs to be known about supports, structures or loads outside the beam segment under consideration.

The beam is quiescent for time $t < 0$, and for $t \geq 0$ it is subjected to a transverse load with finite duration. As a consequence, there will be a deflection of centre-line $w(x,t)$ and a rotation of cross-section $\phi(x,t)$. In the beam segment considered, these deflections and rotations are governed by the equations of motion

$$\frac{\partial Q}{\partial x} = \rho A \frac{\partial^2 w}{\partial t^2}, \; -Q + \frac{\partial M}{\partial x} = \rho I \frac{\partial^2 \phi}{\partial t^2}, \quad (1)$$

Respectively, where $Q(x,t)$ is the transverse shear force and $M(x,t)$ is the bending moment. The deflections and rotations are related to each other through the compatibility-type relation

$$\frac{\partial w}{\partial x} = -\phi + \gamma_0, \qquad (2)$$

Where γ_0 is the shear strain on the centre-line, see Figure 1.

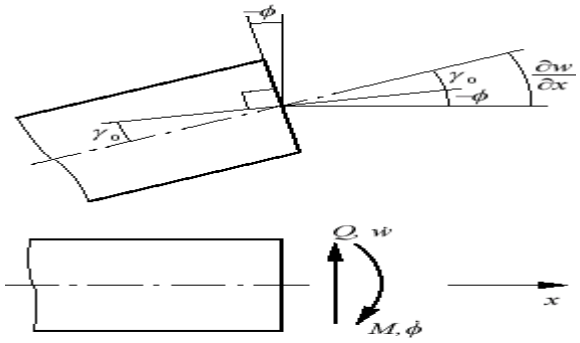

Fig.1. Angles ϕ, γ_0, $\partial w/\partial x$, shear force Q, transverse velocity $\dot{w}$, bending moment M and angular velocity $\dot{\phi}$ at a general section x of the beam.

The terms $-\phi$ and γ_0 on the right-hand side represent the contributions to the slope of the centre-line of the beam from bending and shear, respectively, and they are related to the bending moment and the transverse shear force through the constitutive-type relations

$$M = EI\frac{\partial \phi}{\partial x}, \; Q = \kappa GA\gamma_0, \qquad (3)$$

Where κ is a dimensionless quantity which depends on the shear stress distribution and therefore on the shape of the cross-section. According to beam theory, this quantity can be determined from the relation $\kappa = \left[(A/I^2)\int (S^2/W^2)\mathrm{d}A\right]^{-1}$, where the static moment S and in general also the width W depend on the vertical co-ordinate z from the centre-line. For a rectangular cross-section, this formula gives $\kappa = 5/6 \approx 0.83$, which is the value to be used in the experimental part. According to another definition, κ may depend also on Poisson's ratio.

Equations (1) - (3) provide five relations between the five unknown functions $Q(x,t)$, $w(x,t)$, $M(x,t)$, $\phi(x,t)$ and $\gamma_0(x,t)$. Through elimination, these relations can be transformed into, e.g., a system of two second-order partial differential equations (PDEs) for $w(x,t)$ and $\phi(x,t)$ or into a single fourth-order PDE for $w(x,t)$. Here, it will be more convenient to consider the system of four first-order PDEs

$$\frac{\partial Q}{\partial x}=\rho A\frac{\partial \dot{w}}{\partial t},\ \frac{\partial \dot{w}}{\partial x}=\frac{1}{\kappa GA}\frac{\partial Q}{\partial t}-\dot{\phi},\ \frac{\partial M}{\partial x}=Q+\rho I\frac{\partial \dot{\phi}}{\partial t},\ \frac{\partial \dot{\phi}}{\partial x}=\frac{1}{EI}\frac{\partial M}{\partial t} \qquad (4)$$

For the four quantities $Q(x,t)$, $\dot{w}(x,t)=\partial w(x,t)/\partial t$, $M(x,t)$ and $\dot{\phi}(x,t)=\partial\phi(x,t)/\partial t$, which is obtained by eliminating $\gamma_0(x,t)$ from equations (1) - (3). These quantities constitute the elements of a state vector $\mathbf{s}(x,t)=\left[Q,\dot{w},M,\dot{\phi}\right]^{\mathrm{T}}$, which is zero for $t<0$. Furthermore, because of the energy-absorbing agents outside the beam segment, $\mathbf{s}(x,t)\to\mathbf{0}$ as $t\to\infty$.

The problem to be solved is as follows. Consider the four elements Q, $\dot{w}$, M and $\dot{\phi}$ of the state vector $\mathbf{s}$ at four different sections A, B, C and D of the beam segment, i.e., altogether sixteen elements. Let four out of them, constituting the elements of a vector $\mathbf{m}$, be known from measurements for $t\geq 0$. Then, determine the state vector $\mathbf{s}$ or its Fourier transform $\hat{\mathbf{s}}$ (which is assumed to exist) at any section E of the beam segment. See Figure 2, where it is indicated that the variation of the geometrical and material properties along the beam segment may be continuous or discontinuous

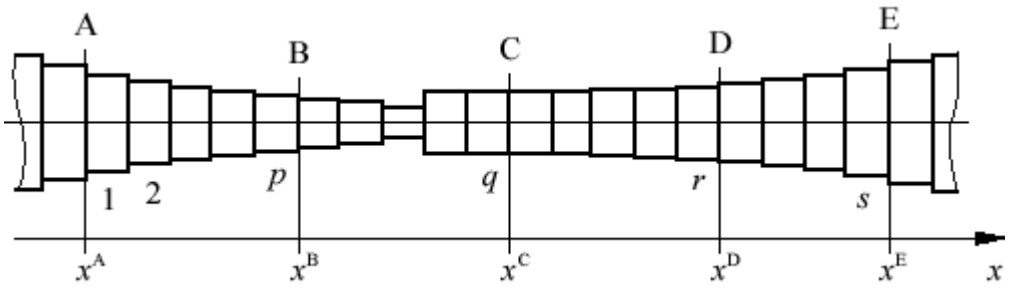

Fig.2 Unloaded section of non-uniform beam in the general case. Sections of measurement A-D and of evaluation E.

B.SOLUTION IN THE GENERAL CASE

Fourier transformation of relations (4) gives $\hat{\mathbf{s}}'=\mathbf{R}\hat{\mathbf{s}}$, (5)

Where

$$\mathbf{R}=\begin{bmatrix}0 & \mathrm{i}\omega\rho A & 0 & 0\\ \mathrm{i}\omega/\kappa GA & 0 & 0 & -1\\ 1 & 0 & 0 & \mathrm{i}\omega\rho I\\ 0 & 0 & \mathrm{i}\omega/EI & 0\end{bmatrix} \qquad (6)$$

Is the system matrix:

$$\hat{\mathbf{s}}=\begin{bmatrix}\hat{Q}\\ \hat{\dot{w}}\\ \hat{M}\\ \hat{\dot{\phi}}\end{bmatrix} \qquad (7)$$

Is the Fourier transform of the state vector $\mathbf{s}$, i.e., $\hat{\mathbf{s}}(x,\omega)=\int_{-\infty}^{\infty}\mathbf{s}(x,t)\,\mathrm{e}^{-\mathrm{i}\omega t}\,\mathrm{d}t$, and $\hat{\mathbf{s}}'=\partial\hat{\mathbf{s}}/\partial x$. The state at any section x is related to that at the fixed section x^0 through

$\hat{\mathbf{s}}(x,\omega)=\mathbf{P}(x,x^0,\omega)\hat{\mathbf{s}}(x^0,\omega)$. (8)

Here, by equations (5) and (8), the transition matrix $\mathbf{P}(x,x^0,\omega)$ satisfies

$\mathbf{P}'=\mathbf{R}\mathbf{P}$, $\mathbf{P}(x^0,x^0,\omega)=\mathbf{I}$, (9)

Where $\mathbf{I}$ is the identity matrix. In particular, equation (8), with $x^0=x^{\mathrm{A}}$ and with $x=x^{\mathrm{A}}$, x^{B}, x^{C}, x^{D} and x^{E}, gives

$\mathbf{P}^{\mathrm{AA}}\hat{\mathbf{s}}^{\mathrm{A}}=\hat{\mathbf{s}}^{\mathrm{A}}$, $\mathbf{P}^{\mathrm{BA}}\hat{\mathbf{s}}^{\mathrm{A}}=\hat{\mathbf{s}}^{\mathrm{B}}$, $\mathbf{P}^{\mathrm{CA}}\hat{\mathbf{s}}^{\mathrm{A}}=\hat{\mathbf{s}}^{\mathrm{C}}$, $\mathbf{P}^{\mathrm{DA}}\hat{\mathbf{s}}^{\mathrm{A}}=\hat{\mathbf{s}}^{\mathrm{D}}$ (10)

For the segments AA, BA, CA and DA, and

$\hat{\mathbf{s}}^{\mathrm{E}}=\mathbf{P}^{\mathrm{EA}}\hat{\mathbf{s}}^{\mathrm{A}}$ (11)

For the segment EA. In equation (10a) it should be noted that $\mathbf{P}^{\mathrm{AA}}=\mathbf{I}$.

The problem of determining the state vector $\hat{\mathbf{s}}^{\mathrm{E}}$ from knowledge of four out of the sixteen elements of the state vectors $\hat{\mathbf{s}}^{\mathrm{A}}$,

$\hat{\mathbf{s}}^{\mathrm{B}}$, $\hat{\mathbf{s}}^{\mathrm{C}}$ and $\hat{\mathbf{s}}^{\mathrm{D}}$ can now be solved as follows. First, four scalar equations, with linear combinations of the elements of $\hat{\mathbf{s}}^{\mathrm{A}}$ in their left-hand members and the measured elements of $\hat{\mathbf{s}}^{\mathrm{A}}$, $\hat{\mathbf{s}}^{\mathrm{B}}$, $\hat{\mathbf{s}}^{\mathrm{C}}$ or $\hat{\mathbf{s}}^{\mathrm{D}}$ in their right-hand members, are singled out from the twelve scalar equations represented by equations (10). They form a system of four linear equations for the four elements of $\hat{\mathbf{s}}^{\mathrm{A}}$ which can, at least in principle, be solved uniquely if the determinant of this system is different from zero. Then, with $\hat{\mathbf{s}}^{\mathrm{A}}$ known, $\hat{\mathbf{s}}^{\mathrm{E}}$ is determined from equation (11). It should be noted that the physical order of sections A-E along the beam must not be alphabetical and also that all sections A-D must not be involved in the measurements.

As a first illustration, consider measurement of the bending moment M at each section A-D. In this case, the third scalar equation from each of the matrix equations (10) gives the system

$$\begin{bmatrix} P_{31}^{\mathrm{AA}} & P_{32}^{\mathrm{AA}} & P_{33}^{\mathrm{AA}} & P_{34}^{\mathrm{AA}} \\ P_{31}^{\mathrm{BA}} & P_{32}^{\mathrm{BA}} & P_{33}^{\mathrm{BA}} & P_{34}^{\mathrm{BA}} \\ P_{31}^{\mathrm{CA}} & P_{32}^{\mathrm{CA}} & P_{33}^{\mathrm{CA}} & P_{34}^{\mathrm{CA}} \\ P_{31}^{\mathrm{DA}} & P_{32}^{\mathrm{DA}} & P_{33}^{\mathrm{DA}} & P_{34}^{\mathrm{DA}} \end{bmatrix} \begin{bmatrix} \hat{Q}^{\mathrm{A}} \\ \hat{w}^{\mathrm{A}} \\ \hat{M}^{\mathrm{A}} \\ \hat{\phi}^{\mathrm{A}} \end{bmatrix} = \begin{bmatrix} \hat{M}_{\mathrm{meas}}^{\mathrm{A}} \\ \hat{M}_{\mathrm{meas}}^{\mathrm{B}} \\ \hat{M}_{\mathrm{meas}}^{\mathrm{C}} \\ \hat{M}_{\mathrm{meas}}^{\mathrm{D}} \end{bmatrix}, \quad (12)$$

Where subscript m denotes measurement. It can also be written

$$\begin{bmatrix} P_{31}^{\mathrm{AA}} & P_{32}^{\mathrm{AA}} & P_{33}^{\mathrm{AA}} & P_{34}^{\mathrm{AA}} \\ P_{31}^{\mathrm{BA}} & P_{32}^{\mathrm{BA}} & P_{33}^{\mathrm{BA}} & P_{34}^{\mathrm{BA}} \\ P_{31}^{\mathrm{CA}} & P_{32}^{\mathrm{CA}} & P_{33}^{\mathrm{CA}} & P_{34}^{\mathrm{CA}} \\ P_{31}^{\mathrm{DA}} & P_{32}^{\mathrm{DA}} & P_{33}^{\mathrm{DA}} & P_{34}^{\mathrm{DA}} \end{bmatrix} \begin{bmatrix} \hat{s}_1^{\mathrm{A}} \\ \hat{s}_2^{\mathrm{A}} \\ \hat{s}_3^{\mathrm{A}} \\ \hat{s}_4^{\mathrm{A}} \end{bmatrix} = \begin{bmatrix} \hat{s}_{3\mathrm{meas}}^{\mathrm{A}} \\ \hat{s}_{3\mathrm{meas}}^{\mathrm{B}} \\ \hat{s}_{3\mathrm{meas}}^{\mathrm{C}} \\ \hat{s}_{3\mathrm{meas}}^{\mathrm{D}} \end{bmatrix}. \quad (13)$$

As $\mathbf{P}^{\mathrm{AA}} = \mathbf{I}$, the first row of the matrix on the left-hand side is $[0,0,1,0]$, which gives the trivial relation $\hat{M}^{\mathrm{A}} = \hat{M}_{\mathrm{meas}}^{\mathrm{A}}$ or $\hat{s}_3^{\mathrm{A}} = \hat{s}_{3\mathrm{meas}}^{\mathrm{A}}$.

As a second illustration, consider measurement of the transverse velocity $\dot{w}$ at each section A-D. In this case, the second scalar equation from each of the matrix equations (10) gives the system

$$\begin{bmatrix} P_{21}^{\mathrm{AA}} & P_{22}^{\mathrm{AA}} & P_{23}^{\mathrm{AA}} & P_{24}^{\mathrm{AA}} \\ P_{21}^{\mathrm{BA}} & P_{22}^{\mathrm{BA}} & P_{23}^{\mathrm{BA}} & P_{24}^{\mathrm{BA}} \\ P_{21}^{\mathrm{CA}} & P_{22}^{\mathrm{CA}} & P_{23}^{\mathrm{CA}} & P_{24}^{\mathrm{CA}} \\ P_{21}^{\mathrm{DA}} & P_{22}^{\mathrm{DA}} & P_{23}^{\mathrm{DA}} & P_{24}^{\mathrm{DA}} \end{bmatrix} \begin{bmatrix} \hat{Q}^{\mathrm{A}} \\ \hat{w}^{\mathrm{A}} \\ \hat{M}^{\mathrm{A}} \\ \hat{\phi}^{\mathrm{A}} \end{bmatrix} = \begin{bmatrix} \hat{\dot{w}}_{\mathrm{meas}}^{\mathrm{A}} \\ \hat{\dot{w}}_{\mathrm{meas}}^{\mathrm{B}} \\ \hat{\dot{w}}_{\mathrm{meas}}^{\mathrm{C}} \\ \hat{\dot{w}}_{\mathrm{meas}}^{\mathrm{D}} \end{bmatrix}, \quad (14)$$

This can also be written

$$\begin{bmatrix} P_{21}^{\mathrm{AA}} & P_{22}^{\mathrm{AA}} & P_{23}^{\mathrm{AA}} & P_{24}^{\mathrm{AA}} \\ P_{21}^{\mathrm{BA}} & P_{22}^{\mathrm{BA}} & P_{23}^{\mathrm{BA}} & P_{24}^{\mathrm{BA}} \\ P_{21}^{\mathrm{CA}} & P_{22}^{\mathrm{CA}} & P_{23}^{\mathrm{CA}} & P_{24}^{\mathrm{CA}} \\ P_{21}^{\mathrm{DA}} & P_{22}^{\mathrm{DA}} & P_{23}^{\mathrm{DA}} & P_{24}^{\mathrm{DA}} \end{bmatrix} \begin{bmatrix} \hat{s}_1^{\mathrm{A}} \\ \hat{s}_2^{\mathrm{A}} \\ \hat{s}_3^{\mathrm{A}} \\ \hat{s}_4^{\mathrm{A}} \end{bmatrix} = \begin{bmatrix} \hat{s}_{2\mathrm{meas}}^{\mathrm{A}} \\ \hat{s}_{2\mathrm{meas}}^{\mathrm{B}} \\ \hat{s}_{2\mathrm{meas}}^{\mathrm{C}} \\ \hat{s}_{2\mathrm{meas}}^{\mathrm{D}} \end{bmatrix}. \quad (15)$$

As $\mathbf{P}^{\mathrm{AA}} = \mathbf{I}$, the first row of the matrix on the left-hand side is $[0,1,0,0]$, which leads to the trivial relation $\hat{\dot{w}}^{\mathrm{A}} = \hat{\dot{w}}_{\mathrm{meas}}^{\mathrm{A}}$ or $\hat{s}_2^{\mathrm{A}} = \hat{s}_{2\mathrm{meas}}^{\mathrm{A}}$.

In the general case, equations (13) and (15) take the form

$$\begin{bmatrix} P_{e_1 1}^{c_1 \mathrm{A}} & P_{e_1 2}^{c_1 \mathrm{A}} & P_{e_1 3}^{c_1 \mathrm{A}} & P_{e_1 4}^{c_1 \mathrm{A}} \\ P_{e_2 1}^{c_2 \mathrm{A}} & P_{e_2 2}^{c_2 \mathrm{A}} & P_{e_2 3}^{c_2 \mathrm{A}} & P_{e_2 4}^{c_2 \mathrm{A}} \\ P_{e_3 1}^{c_3 \mathrm{A}} & P_{e_3 2}^{c_3 \mathrm{A}} & P_{e_3 3}^{c_3 \mathrm{A}} & P_{e_3 4}^{c_3 \mathrm{A}} \\ P_{e_4 1}^{c_4 \mathrm{A}} & P_{e_4 2}^{c_4 \mathrm{A}} & P_{e_4 3}^{c_4 \mathrm{A}} & P_{e_4 4}^{c_4 \mathrm{A}} \end{bmatrix} \begin{bmatrix} \hat{s}_1^{\mathrm{A}} \\ \hat{s}_2^{\mathrm{A}} \\ \hat{s}_3^{\mathrm{A}} \\ \hat{s}_4^{\mathrm{A}} \end{bmatrix} = \begin{bmatrix} \hat{s}_{e_1 \mathrm{meas}}^{c_1} \\ \hat{s}_{e_2 \mathrm{meas}}^{c_2} \\ \hat{s}_{e_3 \mathrm{meas}}^{c_3} \\ \hat{s}_{e_4 \mathrm{meas}}^{c_4} \end{bmatrix} \quad (16)$$

Or

$$\mathbf{M}\hat{\mathbf{s}}^{\mathrm{A}} = \hat{\mathbf{m}}, \quad (17)$$

Where

$$M_{jk} = P_{e_j k}^{c_j \mathrm{A}}, \ \hat{m}_j = \hat{s}_{e_j \mathrm{meas}}^{c_j}. \quad (18)$$

Here $\mathbf{M}$ is a matrix with elements M_{jk} singled out from the transition matrices $\mathbf{P}^{\mathrm{AA}}$, $\mathbf{P}^{\mathrm{BA}}$, $\mathbf{P}^{\mathrm{CA}}$ and $\mathbf{P}^{\mathrm{DA}}$, and $\hat{\mathbf{m}}$ is a vector with elements $\hat{m}_j$ of measured quantities at different sections of the beam (j and $k = 1, 2, 3$ or 4). The subscript $e_j = 1, 2, 3$ or 4 defines the type of quantity ($\hat{Q}$, $\hat{w}$, $\hat{M}$ or $\hat{\phi}$, respectively) and the superscript $c_j =$ A, B, C or D the section associated with $\hat{m}_j$. These quantities, which can be considered to be the elements of vectors $\mathbf{e}$ and $\mathbf{c}$, respectively, define the measurements.

Equations (11) and (17) give the state vector

$$\hat{\mathbf{s}}^{\mathrm{E}} = \mathbf{P}^{\mathrm{EA}}\mathbf{M}^{-1}\hat{\mathbf{m}}, \quad (19)$$

in terms of the vector $\hat{\mathbf{m}}$ of measured quantities. Transformation into the time domain gives the state vector $\mathbf{s}^{\mathrm{E}}(t)$ for $t \geq 0$. This solves the stated problem.

If there is an error $\Delta\hat{\mathbf{m}}$ in $\hat{\mathbf{m}}$, it follows that there will be a corresponding error

$$\Delta\hat{\mathbf{s}}^{\mathrm{E}} = \mathbf{P}^{\mathrm{EA}}\mathbf{M}^{-1}\Delta\hat{\mathbf{m}} \quad (20)$$

in $\hat{\mathbf{s}}^{\mathrm{E}}$. On the element level, an error $\Delta\hat{s}_j^{\mathrm{E}}$ in the evaluated quantity $\hat{s}_j^{\mathrm{E}}$, due to an error $\Delta\hat{m}_k$ in the measured quantity $\hat{m}_k$, can be expressed $\Delta\hat{s}_j^{\mathrm{E}} = \left(\partial\hat{s}_j^{\mathrm{E}} / \partial\hat{m}_k\right)\Delta\hat{m}_k$. Comparison with equation (20) shows that the derivative $\partial\hat{s}_j^{\mathrm{E}} / \partial\hat{m}_k$ can be obtained as the element jk of the matrix $\mathbf{P}^{\mathrm{EA}}\mathbf{M}^{-1}$. The absolute value of this derivative will be used as a measure of the sensitivity of the evaluated quantity $\hat{s}_j^{\mathrm{E}}$ to an error in the measured quantity $\hat{m}_k$.

C.BEAM WITH PIECEWISE CONSTANT PROPERTIES

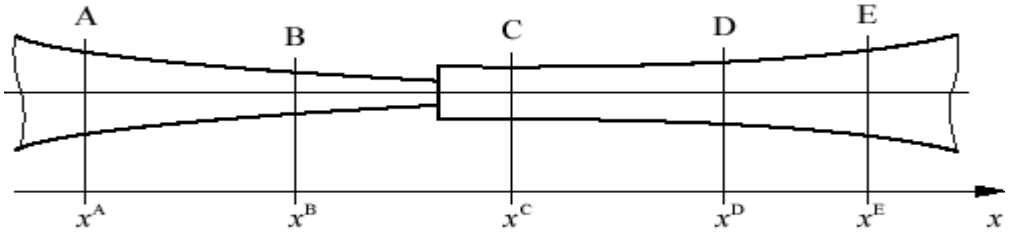

Fig.3 Unloaded section of beam with piece-wise constant properties. Sections of measurement A-D and of evaluation E.

If the beam has piecewise constant properties as indicated in Figure 3, the transition matrices in equations (10b-d) and (11) can be expressed as the products

$$\mathbf{P}^{\mathrm{BA}} = \mathbf{P}^{p}\mathbf{P}^{p-1}\ldots\mathbf{P}^{1}, \ \mathbf{P}^{\mathrm{CA}} = \mathbf{P}^{q}\mathbf{P}^{q-1}\ldots\mathbf{P}^{1}, \ \mathbf{P}^{\mathrm{DA}} = \mathbf{P}^{r}\mathbf{P}^{r-1}\ldots\mathbf{P}^{1}, \quad (21)$$

And

$$\mathbf{P}^{\mathrm{EA}} = \mathbf{P}^{s}\mathbf{P}^{s-1}\ldots\mathbf{P}^{1}, \quad (22)$$

Respectively, of transition matrices $\mathbf{P}^{1}$, $\mathbf{P}^{2}$,..., $\mathbf{P}^{s}$ for beam elements with constant properties. These matrices, in turn, can be determined by first solving the problem (9) for matrices $\mathbf{R}$ which are independent of x, and then substituting appropriate values for x and x^{0}. In this case, the coupled problem (9) for the elements of $\mathbf{P}$ can be replaced by an uncoupled problem as follows.

For $\mathbf{R}$ independent of x, equation (9a) gives

$$\mathbf{P}' = \mathbf{RP}\,, \quad \mathbf{P}'' = \mathbf{R}^2\mathbf{P}\,, \quad \mathbf{P}''' = \mathbf{R}^3\mathbf{P}\,, \quad \mathbf{P}^{\mathrm{IV}} = \mathbf{R}^4\mathbf{P}\,. \quad (23)$$

The eigenvalues γ of the matrix $\mathbf{R}$ are given by the four roots of $|\mathbf{R} - \gamma\mathbf{I}| = 0$, i.e., with use of definition (6),

$$\gamma^4 + 2a\gamma^2 - b = 0\,, \quad (24)$$

Where

$$a = \frac{\rho\omega^2}{2E}\left(1 + \frac{E}{\kappa G}\right), \quad b = \frac{\rho A\omega^2}{EI}\left(1 - \frac{\rho I\omega^2}{\kappa GA}\right). \quad (25)$$

Thus, there are the two pairs of eigenvalues

$$\gamma = \pm\alpha\,, \ \gamma = \pm ik\,, \quad (26)$$

Where

$$\alpha = \left[\left(b + a^2\right)^{1/2} - a\right]^{1/2}, \quad k = \left[\left(b + a^2\right)^{1/2} + a\right]^{1/2} \quad (27)$$

Are both real and positive provided that

$$|\omega| < \left(\frac{\kappa GA}{\rho I}\right)^{1/2}, \quad (28)$$

Which is presumed. According to Cayley-Hamilton's theorem, equation (24) for the eigenvalues of the matrix $\mathbf{R}$ is satisfied also by $\mathbf{R}$, i.e.,

$$\mathbf{R}^4 + 2a\mathbf{R}^2 - b\mathbf{I} = \mathbf{0}\,. \quad (29)$$

Multiplication by $\mathbf{P}$ from the right and use of relations (23b, d) gives the fourth-order differential equation

$$\mathbf{P}^{\mathrm{IV}} + 2a\mathbf{P}'' - b\mathbf{P} = \mathbf{0}\,. \quad (30a)$$

Furthermore, relations (9b) and (23a-c) give the conditions

$$\mathbf{P}(x^0, x^0, \omega) = \mathbf{I}\,, \quad (30b)$$

$$\mathbf{P}'(x^0, x^0, \omega) = \mathbf{R}\,, \ \mathbf{P}''(x^0, x^0, \omega) = \mathbf{R}^2\,, \quad \mathbf{P}'''(x^0, x^0, \omega) = \mathbf{R}^3 \ (30c\text{-}e)$$

For $x = x^0$. Thus, the coupled problem (9) for the elements of $\mathbf{P}$ has been replaced by the uncoupled problem (30), which has the solution

$$\mathbf{P}(x, x^0, \omega) = \mathbf{A}\cos\left[k(x - x^0)\right] + \mathbf{B}\sin\left[k(x - x^0)\right] + \mathbf{C}\cosh\left[\alpha(x - x^0)\right] + \mathbf{D}\sinh\left[\alpha(x - x^0)\right] \quad (31)$$

With

$$\mathbf{A} = \frac{1}{\alpha^2 + k^2}\left(\alpha^2\mathbf{I} - \mathbf{R}^2\right), \ \mathbf{B} = \frac{1}{k(\alpha^2 + k^2)}\left(\alpha^2\mathbf{R} - \mathbf{R}^3\right), \quad (32a, b)$$

$$\mathbf{C} = \frac{1}{\alpha^2 + k^2}\left(k^2\mathbf{I} + \mathbf{R}^2\right), \ \mathbf{D} = \frac{1}{\alpha(\alpha^2 + k^2)}\left(k^2\mathbf{R} + \mathbf{R}^3\right) \quad (32c, d)$$

III.EXPERIMENTAL TESTS

The experimental set-up is illustrated in Figure 4. A beam made of aluminium (AA 6061-T6; $E = 70$ GPa, $\nu = 0.3$ and $\rho = 2700$ kg/m^3) with rectangular cross-section and length 2250 mm was used. The width W of the beam was 20 mm, while its height H was 15 mm in the central third and 20 mm in the two outer thirds. The beam was held in position by three supports with positions as shown. Each of these supports was realised with a pair of 15 mm wide clamps clad with 1.5 mm thick rubber plates. The beam was impacted laterally by a spherical steel ball which was guided by a tube and dropped from a height of 600 mm. The diameter of the ball was 50 mm, and its mass was 535 g. A 3 mm thick rubber plate at the impacted spot of the beam served to reduce the excitation at high frequencies.

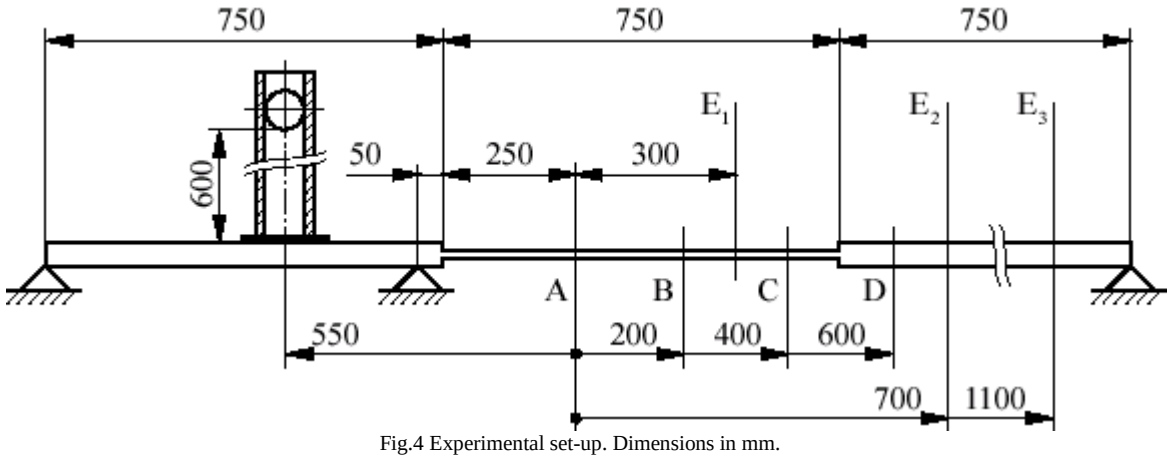

Fig.4 Experimental set-up. Dimensions in mm.

The beam was instrumented with strain gauges and accelerometers at the sections A-D and E_1-E_3 as shown in Figure 4. The positions of the strain gauges coincided with these sections, while those of the accelerometers were displaced 20 mm to the right, i.e., away from the spot of impact. The strain gauges (TML FLA-5-23-1L) were glued (Tokyo Sokki Kenkyujo Co, Ltd, Adhesive CN) to the beam

in pairs with one on the top and one on the bottom. The gauges of each pair were connected to a bridge amplifier (Measurement Group 2210) in opposite branches, so that the output of the amplifier was proportional to the difference between the two strains, and therefore to the bending moment M at the section. Shunt calibration was used. Accelerometers (Brüel & Kjær, three Types 4374 and two Type 4393) were attached with thin layers of wax. The accelerometers were connected to charge amplifiers (three Kistler Type 5011 and two Brüel & Kjær Type 2635). Ideally, there should have been one type of accelerometer and one type of charge amplifier only, but it was judged that the use of different types would not have any noticeable effect upon the results.

The amplified strain and accelerometer signals were fed to analogue aliasing filters (DIFA Measuring Systems, PDF) with cut-off frequency 17.5 kHz. The filtered signals were recorded in a time interval $[0, t_{\mathrm{re}}]$, with $t_{\mathrm{re}} \approx 0.25$ s, by two synchronised four-channel digital oscilloscopes (Nicolet Pro 20 and Pro 40) which used a sampling interval of 20 μs. At the end of this time interval, the amplitudes of the recorded signals were reduced to about a tenth due to the damping action of the supports. The recorded signals were transferred to a computer for evaluation of the state vector $\mathbf{s}^{\mathrm{E}}(t)$. First, measured accelerations, if any, were integrated to velocities. After use of the FFT algorithm, $\hat{\mathbf{s}}^{\mathrm{E}}(\omega)$ was determined according to equation (19). Finally, $\hat{\mathbf{s}}^{\mathrm{E}}(\omega)$ was transformed into the time domain by use of the inverse FFT algorithm. Results were produced for the same time interval $[0, t_{\mathrm{re}}]$ even though sometimes they may be valid only in a narrower interval $[0, t_{\mathrm{ev}}]$. When, e.g., section E is located outside AD, as in some of the experimental tests, there must clearly be a certain difference between t_{re} and t_{ev} which is related to the travel times for flexural waves from section E to sections A-D.

Four test cases, labelled 1 - 4, are defined in Table 1. In Case 1, bending moments M at sections A-D ($\mathbf{e} = [3,3,3,3]^{\mathrm{T}}$, $\mathbf{c} = [\mathrm{A,B,C,D}]^{\mathrm{T}}$) and E_1-E_3 were determined from measurements of strains at the same sections. In Case 2, bending moments M at sections A-D and transverse velocities $\dot{w}$ at E_1-E_3 were determined from measurements of strains and accelerations, respectively, at the same sections. In Case 3, transverse velocities $\dot{w}$ at sections A-D ($\mathbf{e} = [2,2,2,2]^{\mathrm{T}}$, $\mathbf{c} = [\mathrm{A,B,C,D}]^{\mathrm{T}}$) and E_2 were determined from measurements of accelerations at the same sections. In Case 4, finally, transverse velocities $\dot{w}$ at sections A-D and bending moment M at E_2 were determined from measured accelerations and strains, respectively, at the same sections. In this case, the signals representing accelerations and strains were passed through 8-pole Butterworth high-pass filters with cut-off frequency 10 Hz. In each of the four cases, bending moments M or transverse velocities $\dot{w}$ at sections E_1-E_3, corresponding to the measurements made at these sections, were also determined from those measured at A-D according to equation (19). All tests were carried out at room temperature.

TABLE I CASES OF EXPERIMENTAL TESTS.

Case	Input A-D	Output			High-pass Filter
		E_1	E_2	E_3	
1	M	M	M	M	No
2	M	$\dot{w}$	$\dot{w}$	$\dot{w}$	No
3	$\dot{w}$	-	$\dot{w}$	-	No
4	$\dot{w}$	-	M	-	Yes

IV. RESULTS

Figure 5 shows for Case 1 the sensitivity $\left|\partial \hat{M}^{\mathrm{E}} / \partial \hat{M}^{\mathrm{C}}\right|$ of the bending moment $\hat{M}^{\mathrm{E}}$ to an error in the bending moment $\hat{M}^{\mathrm{C}}$ as a function of the position x^{E} of section E and of the frequency $f = \omega / 2\pi$. It can be seen that the sensitivity to error is unity or less if the position x^{E} is not too far outside the interval $[x^{\mathrm{A}}, x^{\mathrm{D}}]$ and if the frequency is not too high. In particular, the sensitivity to error is zero if $x^{\mathrm{E}} = x^{\mathrm{A}}$, x^{B} or x^{D}, and it is unity if $x^{\mathrm{E}} = x^{\mathrm{C}}$. It should also be noted that the sensitivity to error is very high around a frequency of approximately 850 Hz. Similar results were obtained for other cases and other sensitivities.

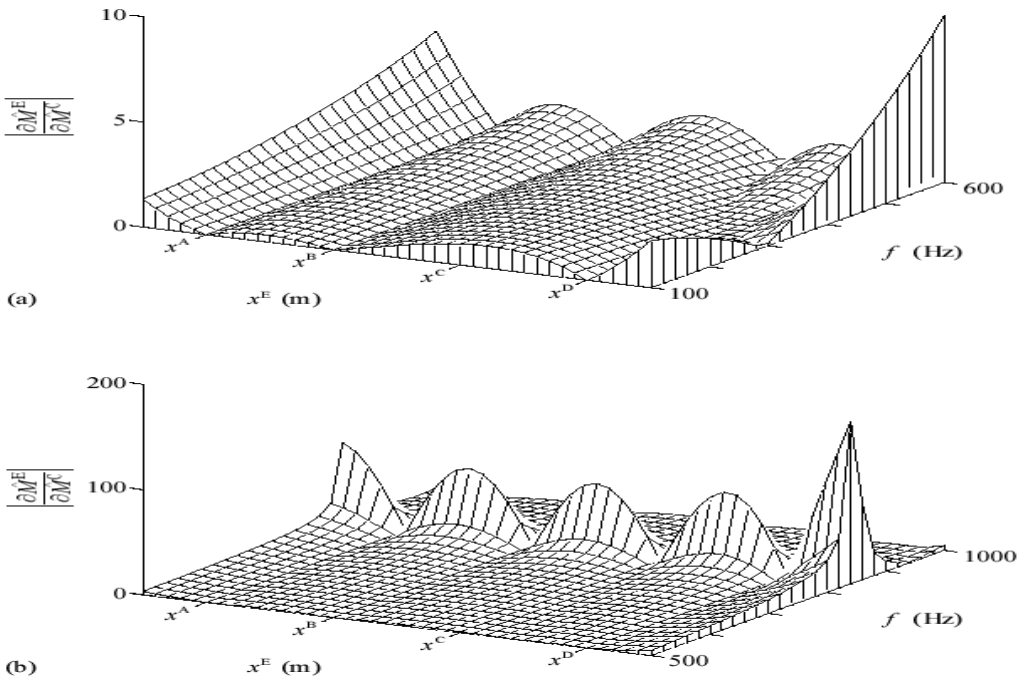

Fig.5 Sensitivity $\left|\partial \hat{M}^{\mathrm{E}} / \partial \hat{M}^{\mathrm{C}}\right|$ of bending moment $\hat{M}^{\mathrm{E}}$ to error in bending moment $\hat{M}^{\mathrm{C}}$ vs. position x^{E} and frequency f in Case 1. (a) 100 Hz $< f <$ 600 Hz and (b) 500 Hz $< f <$ 1000 Hz.

Figure 6 shows results in the time and frequency domains at section E_1 for Case 1. In Figure 6(a), the results in the time domain are based on frequencies up to 500 Hz, which means that frequencies around 850 Hz are excluded, while in Figure 6(b) they are based on frequencies up to 2000 Hz. Evidently, there is a significantly better agreement between evaluated and measured bending moments in the former case. For this reason, the results for Cases 1-4 shown in Figures 7-10 are based on frequencies up to 500 Hz.

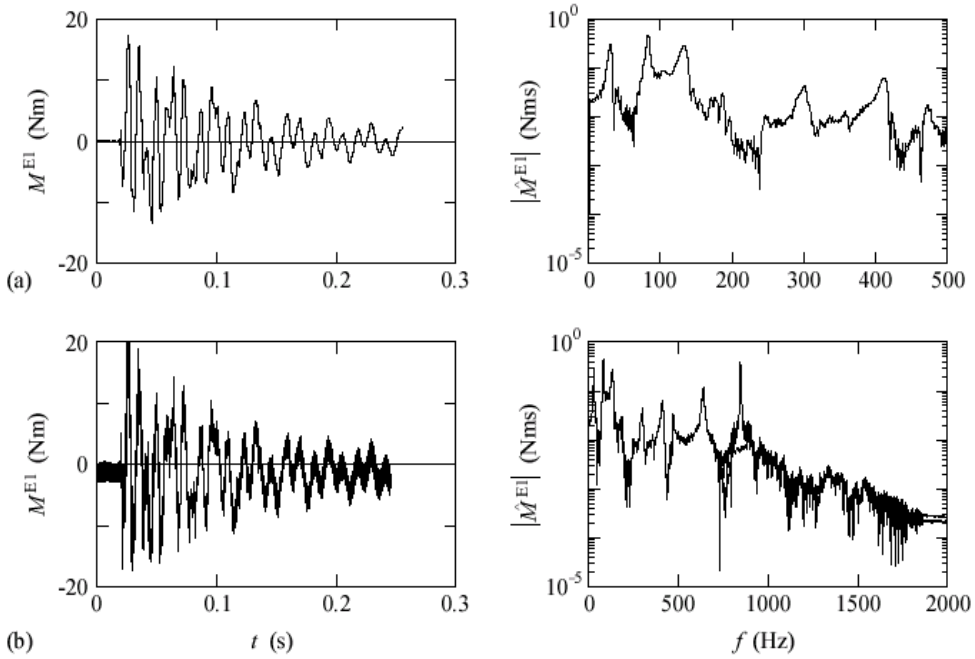

Fig.6. Bending moment M^{E1} vs. time t and $\left|\hat{M}^{\mathrm{E1}}\right|$ vs. frequency f. Comparison between bending moment at E_1 evaluated from bending moments measured at A-D (solid curves) and bending moment measured at E_1 (dotted curves) in Case 1. Results for frequencies up to (a) 500 Hz and (b) 2000 Hz.

V. DISCUSSIONS

It has been shown how the elements Q, $\dot{w}$, M and $\dot{\phi}$ of the state vector $\mathbf{s}$ at any section E of an unloaded segment of a non-uniform beam can be determined from measurement of four such elements at up to four different sections A, B, C and D of the same unloaded segment of the beam. This has also been demonstrated experimentally. Once the state vector has been determined, several quantities of importance can be obtained from its elements. Thus, e.g., the shear stress τ can be obtained from Q, the normal stress σ from M, the deflection w from $\dot{w}$, and the rotation of the cross-section ϕ from $\dot{\phi}$. Also, the power transmission can be obtained from the relation $P = -(Q\dot{w} + M\dot{\phi})$. It should be emphasized that nothing needs to be known about supports, structures and loads outside the beam segment under consideration.

The combination of sections, among A, B, C and D, and types of quantities to be measured, among Q, $\dot{w}$, M and $\dot{\phi}$, can be chosen in a large number of ways, some of which may be more interesting than others. Thus, it is convenient to determine bending moment M from measured strains and transverse velocity $\dot{w}$ from measured accelerations, as was done in the experimental part, while it is less straightforward to determine Q or $\dot{\phi}$ from measurements. Also, it seems preferable to place at most two types of transducers at any section A-D of the beam, and to make the same kind of measurement or measurements at each instrumented section. Therefore, two interesting possibilities are measurement of (i) M at each section A-D (Cases 1-2) and (ii) $\dot{w}$ at each section A-D (Cases 3-4), as in the experimental part. A third interesting possibility would be measurement of (iii) both M and $\dot{w}$ at each of two sections, e.g., A and B. It should also be noted, that a free end, say A, with $Q^{\mathrm{A}} \equiv 0$ and $M^{\mathrm{A}} \equiv 0$ can be used to replace two measurements. Other types of homogeneous boundary conditions generally represent real situations less accurately.

The functions $\alpha(\omega)$ and $k(\omega)$ introduced in equations (26) and (27) can be interpreted as follows. Let the state vector have the form $\hat{\mathbf{s}} = \hat{\mathbf{s}}^* \exp(\beta x)$. Then, substitution into equation (5) gives the eigenvalue problem $\mathbf{R}\hat{\mathbf{s}}^* = \beta\hat{\mathbf{s}}^*$. The eigenvalues β are given by the four roots of $|\mathbf{R} - \beta\mathbf{I}| = 0$, i.e., the four roots of equation (24) with $\beta = \gamma$. Thus, according to equation (26), the eigenvalues are $\beta = \pm\alpha$ and $\beta = \pm ik$. Therefore, provided that the condition (28) is satisfied as presumed, α determines the decay of non-propagating disturbances and k is the wave number of propagating harmonic waves ($\omega > 0$).

For radian frequencies $|\omega| << \omega_0 = c_0 / R$, where $c_0 = (E/\rho)^{1/2}$ is the speed of elastic extensional waves and $R = (I/A)^{1/2}$ is the radius of inertia of the cross-section, equations (27) can be approximated by $\alpha \approx k \approx b^{1/4}$ and equation (25b) by $b \approx (\rho A/EI)\omega^2$. As by definition the wave number k is related to the wave length λ by $k = 2\pi/\lambda$, one obtains $\alpha \approx 2\pi/\lambda$ with $\lambda \approx 2\pi(c_0 R/|\omega|)^{1/2} >> 2\pi R$. In terms of the frequency $f = \omega/2\pi$ and the height $H = 2\sqrt{3}R$ of a beam with rectangular cross section, the corresponding relations are $|f| << f_0 = c_0/\theta H$, $\alpha \approx 2\pi/\lambda$, and $\lambda \approx (c_0\theta H/|f|)^{1/2} >> \theta H$, with $\theta = \pi/\sqrt{3}$. These approximations of α and λ at low frequencies represent the limiting case of the Euler-Bernoulli beam.

For the aluminium beam used in the experimental tests, the highest frequency normally considered, 500 Hz, corresponds to the wavelengths 0.606 m and 0.525 m in the segments with heights 20 mm and 15 mm, respectively. Similarly, the frequency 2000 Hz, considered in Figure 6 only, corresponds to the wavelengths 0.300 m and 0.260 m, respectively. Thus, in the tests carried out the wavelengths were much larger than the heights of the beam, and $|f| << f_0$. This means that the above approximations are accurate and also that the condition (28), which can be written in the form $f < f_0[\kappa/2(1+\nu)]^{1/2}$, is satisfied.

The determination of errors at section E due to errors of measurement, including noise, at one or several of sections A-D according to relation (20) can be split into the two steps (i) $\Delta\hat{\mathbf{s}}^{\mathrm{A}} = \mathbf{M}^{-1}\Delta\hat{\mathbf{m}}$, which gives errors at section A in terms of errors of measurement, and (ii) $\Delta\hat{\mathbf{s}}^{\mathrm{E}} = \mathbf{P}^{\mathrm{EA}}\Delta\hat{\mathbf{s}}^{\mathrm{A}}$, which gives errors at E in terms of errors at A. In the time domain, these steps correspond to a deconvolution and a convolution, respectively. Under certain conditions, each of them may generate large errors. Such conditions are related to the matrices $\mathbf{P}^{\mathrm{AA}}$ - $\mathbf{P}^{\mathrm{DA}}$, which determine the elements of the matrix $\mathbf{M}$, and to the matrix $\mathbf{P}^{\mathrm{EA}}$. For the discussion which follows it is useful to note from equation (31) that, in the special case of a uniform beam and for relatively low frequencies with $\alpha \approx 2\pi/\lambda$, these matrices contain terms proportional to e^0, $e^{\pm 2\pi(x_{\mathrm{B}} - x_{\mathrm{A}})/\lambda}$, ..., and $e^{\pm 2\pi(x_{\mathrm{E}} - x_{\mathrm{A}})/\lambda}$, respectively.

In the first step, which involves inversion of the matrix $\mathbf{M}$, the error $\Delta\hat{\mathbf{s}}^{\mathrm{A}}$ may become large if the matrix $\mathbf{M}$ is ill-conditioned. In the case represented by equation (12), this may occur at low frequencies corresponding to long wave lengths which make the four scalar equations nearly the same. It may also occur at high frequencies corresponding to short wave lengths which make the magnitudes of the elements in the different rows of the matrix $\mathbf{M}$ very different. Thus, e.g., the ratio of the exponential factors of the fourth row in equation (12) to those of the first row is

$e^{2\pi(x_D - x_A)/\lambda}$, which may be very large even for modest ratios $(x_D - x_A)/\lambda > 1$. In the experimental tests, the distance AD (600 mm) was slightly longer than one wave length ($\approx 1.12\lambda$) at the highest frequency 500 Hz which corresponds to the ratio $e^{2.24\pi} \approx 1.1 \cdot 10^3$. The matrix $\mathbf{M}$ may be ill-conditioned also near discrete frequencies which make several distances between adjacent sections A-D equal to an integral multiple of a half wave length. In Case 1, the distances AB and BC in the thinner central section of the beam are one half wave length at a frequency of about 860 Hz which may explain the high sensitivity to errors around 850 Hz illustrated in Figure 5. This problem was avoided in the experimental tests by only considering frequencies below 500 Hz. The effects of noise in the measured data may be reduced by use of Wiener filtering techniques [16]. Also, a conceivable way of avoiding integral multiples of half wave lengths between adjacent sections A-D, which might allow frequencies considerably higher than 500 Hz, would be to make use of more than four measurements, so that the system (17) for the elements of $\hat{\mathbf{s}}^{\mathrm{A}}$ would be over-determined, and of a non-uniform distribution of instrumented sections. This way of eliminating critical frequencies has been found to be effective in an application involving viscoelastic extensional waves [17].

In the second step, which involves multiplication of the error $\Delta\hat{\mathbf{s}}^{\mathrm{A}}$ at section A with the matrix $\mathbf{P}^{\mathrm{EA}}$, the error $\Delta\hat{\mathbf{s}}^{\mathrm{E}}$ may become large if the exponential factor $e^{2\pi(x_{\mathrm{E}} - x_{\mathrm{A}})/\lambda}$ is very large. This occurs if the distance AE is large. In the experimental tests the distances AE_1, AE_2 and AE_3 were approximately 0.57, 1.28 and 1.94 wave lengths at the highest frequency 500 Hz. Thus, E_1 was located at the centre of the beam segment AD, while E_2 and E_3 were located at distances 0.16 and 0.82 wave lengths, respectively, outside this segment. The corresponding exponential factors were $e^{1.14\pi} \approx 3.6 \cdot 10^1$, $e^{2.56\pi} \approx 3.1 \cdot 10^3$ and $e^{3.88\pi} \approx 2.0 \cdot 10^5$, respectively. For Case 1, Figure 7 shows that there is excellent agreement in the frequency range 2-500 Hz between (i) the bending moment evaluated at section E_1 from measurements of bending moments at sections A-D and (ii) the bending moment measured at the same section E_1. For section E_2 the agreement is very good in the same range of frequencies. For section E_3 there is relatively large disagreement, in particular at high frequencies, corresponding to short wave lengths and large exponential factors $e^{2\pi(x_{\mathrm{E}} - x_{\mathrm{A}})/\lambda}$, and in the time domain near $t \approx t_{\mathrm{re}} \approx 0.25$ s.

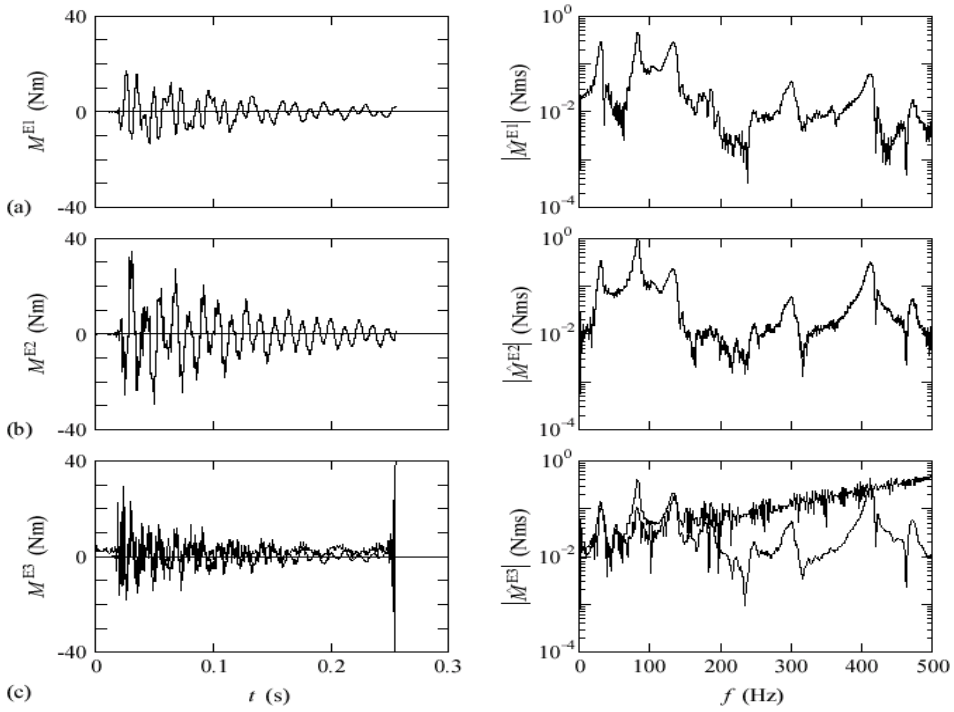

Fig.7. Bending moments (a) M^{E1} vs. time t and $\left|\hat{M}^{\mathrm{E1}}\right|$ vs. frequency f, (b) M^{E2} vs. time t and $\left|\hat{M}^{\mathrm{E2}}\right|$ vs. frequency f, and (c) M^{E3} vs. time t and $\left|\hat{M}^{\mathrm{E3}}\right|$ vs. frequency f. Comparison between bending moments at E_1 - E_3 evaluated from bending moments measured at A-D (solid curves) and bending moment measured at E_1 - E_3 (dotted curves) in Case 1. Results for frequencies up to 500 Hz.

For Case 2, Figure 8 shows that there is good agreement in the frequency range 10-500 Hz between (i) the transverse velocity evaluated at section E_1 from measurements of bending moments at sections A-D and (ii) the transverse velocity measured at the same section E_1. For section E_2 the agreement is fair in the same range of frequencies. For section E_3 there is again relatively large disagreement, in particular at high frequencies, corresponding to short wave lengths and large exponential factors $e^{2\pi(x_{\mathrm{E}}-x_{\mathrm{A}})/\lambda}$, and in the time domain near $t \approx t_{\mathrm{re}} \approx 0.25$.

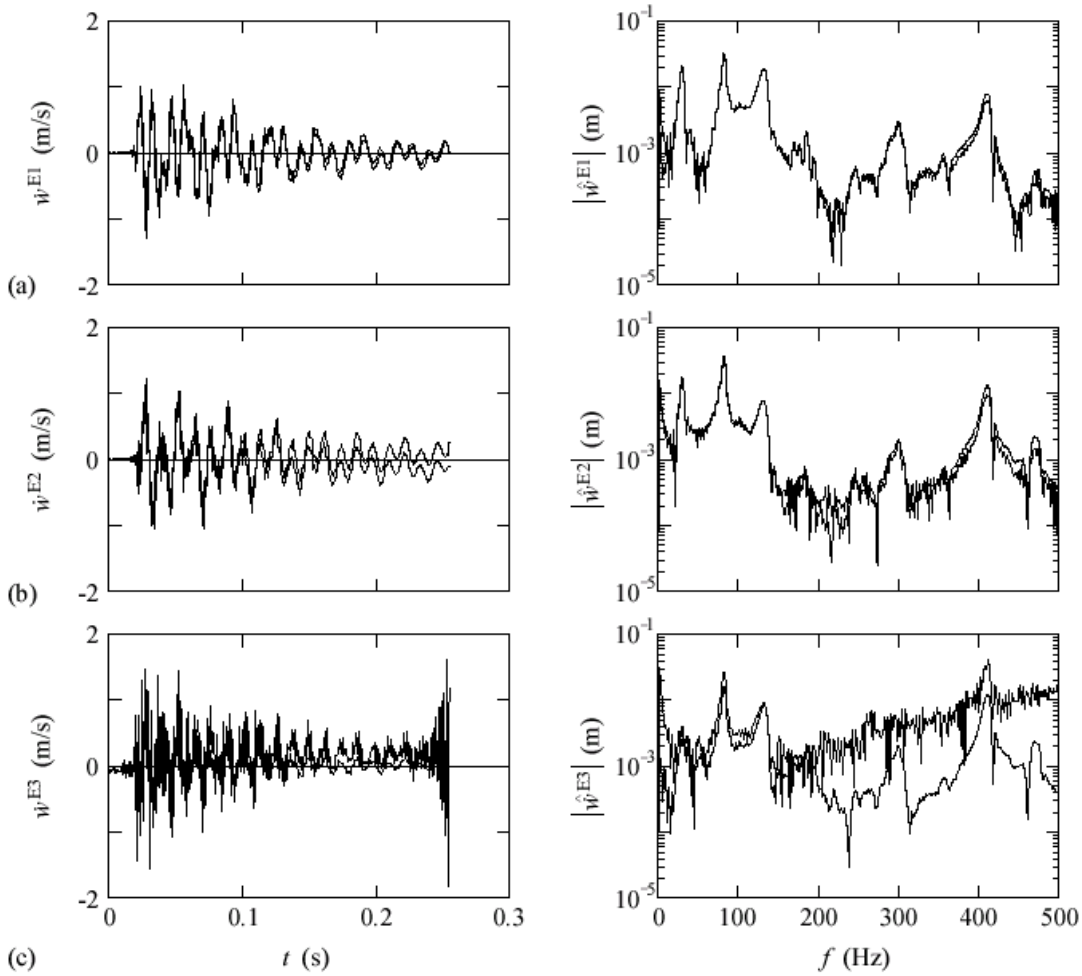

Fig.8. Transverse velocities (a) $\dot{w}^{\mathrm{E1}}$ vs. time t and $\left|\hat{\dot{w}}^{\mathrm{E1}}\right|$ vs. frequency f, (b) $\dot{w}^{\mathrm{E2}}$ vs. time t and $\left|\hat{\dot{w}}^{\mathrm{E2}}\right|$ vs. frequency f, and (c) $\dot{w}^{\mathrm{E3}}$ vs. time t and $\left|\hat{\dot{w}}^{\mathrm{E3}}\right|$ vs. frequency f. Comparison between transverse velocities at E_1 - E_3 evaluated from bending moments measured at A-D (solid curves) and transverse velocities measured at E_1 - E_3 (dotted curves) in Case 2. Results for frequencies up to 500 Hz.

Cases 1 and 2 show that the quality of the evaluated results is generally high when section E is located within the segment AD, whereas it rapidly decays outside. This is consistent with the rapid increase in sensitivity to errors outside the segment AD shown in Figure 5 for Case 1. The large disagreement near $t \approx t_{\mathrm{re}} \approx 0.25$ s for section E_3 in both cases is believed to be due to the difference between t_{re} and t_{ev} which was mentioned in the experimental part. Thus, where the large errors occur, information from section E_3 may not yet have reached sections A-D to the extent required. This error can be avoided by recording signals till all waves are damped out. Then, t_{re} and t_{ev} can be considered to be arbitrarily large.

For Case 3, Figure 9 shows that there is a fair agreement in the frequency range 20-500 Hz between (i) the transverse velocity evaluated at section E_2 from measurements of transverse velocities at sections A-D and (ii) the transverse velocity measured at the same section E_2. For Case 4, Fig-

ure 10 shows that there is a fair agreement in the same range of frequencies between (i) the bending moment evaluated at section E_2 from measurements of transverse velocities at sections A-D and (ii) the bending moment measured at the same section E_2.

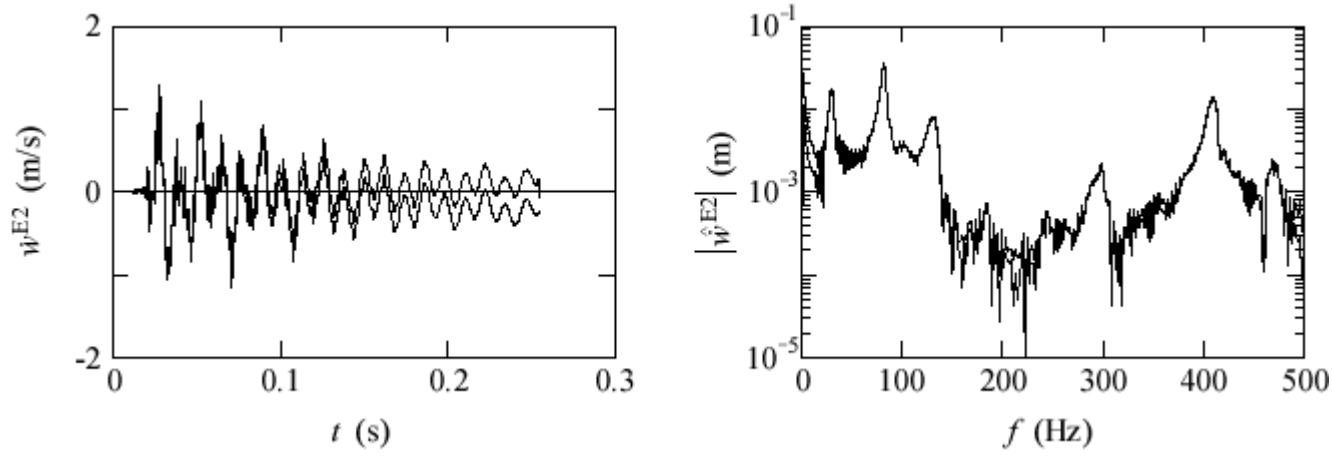

Fig.9 Transverse velocity $\dot{w}^{E2}$ vs. time t and $|\hat{\dot{w}}^{E2}|$ vs. frequency f. Comparison between transverse velocity at E_2 evaluated from transverse velocities measured at A-D (solid curves) and transverse velocity measured at E_2 (dotted curves) in Case 3. Results for frequencies up to 500 Hz.

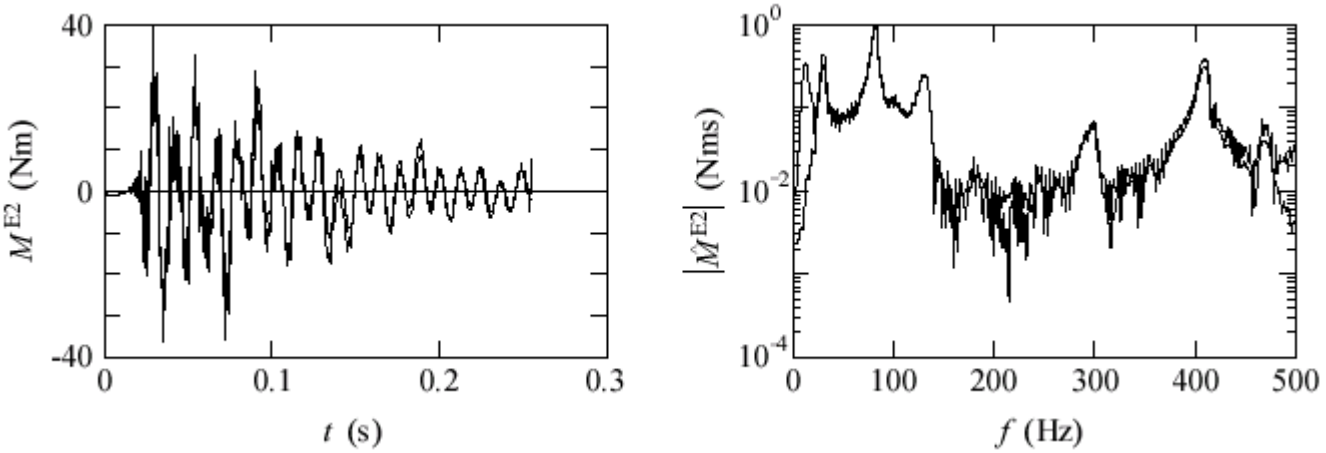

Fig.10 Bending moment M^{E2} vs. time t and $|\hat{M}^{E2}|$ vs. frequency f. Comparison between bending moment evaluated at E_2 from transverse velocities measured at A-D (solid curves) and bending moment measured at E_2 (dotted curves) in Case 4. Results for frequencies up to 500 Hz.

It should be noted that the accelerometers used are quite inaccurate below 10 Hz. This inaccuracy is reflected by the disagreement between evaluated and measured quantities below 10-20 Hz in Cases 2-4. The fair agreement in Case 4 was obtained by using the Butterworth high-pass filters which reduced this disagreement.

Comparison of Figures 7(b) and 10 shows that the bending moment evaluated at section E_2 is more accurate if the evaluation is based on measured bending moments at sections A-D than on measured transverse velocities. Similarly, comparison of Figures 8(b) and 9 shows that the transverse velocity evaluated at section E_2 is more accurate if the evaluation is based on measured transverse velocities at A-D than on measured bending moments. This is partly explained by Figure 6 which shows that when the quantity evaluated at E is the same as that measured at A-D, the sensitivity to errors is relatively low within and near the segment AD of the beam. This is not necessarily the case when the quantity evaluated at E is different from that (or those) measured at A-D. The method of this paper makes use of transition matrices which relate the state vectors at the two ends of a beam element. It would be possible, as an alternative, to make use of the corresponding dynamic stiffness matrices which relate the generalised forces to the generalised velocities at the two ends of the beam element. For the beam segment considered, this approach would result in a

system $\mathbf{Zv} = \mathbf{F}$, where $\mathbf{Z}$ is the dynamic stiffness matrix, $\mathbf{v}$ is the nodal generalised velocity vector, and $\mathbf{F}$ is the nodal generalised load vector. If the number of nodes of the beam segment considered would be n, corresponding to $n-1$ beam elements, the matrix $\mathbf{Z}$ would be $2n \times 2n$ and the vector $\mathbf{v}$ would contain $2n$ generalised velocities (n velocities and n angular velocities). Also, the vector $\mathbf{F}$ would contain four nodal generalised forces (one transverse shear force and one bending moment at each end node of the beam segment considered) in addition to zeroes. Thus, there would be a system of $2n$ relations between $2n+4$ generalised velocities and forces. If four of these quantities are measured, the system $\mathbf{Zv} = \mathbf{F}$ can generally be solved for the remaining ones. Although there may be differences in ease of establishing the system to be solved, in ease of obtaining the desired elements of the state vector, in ease of interpretation of the wave phenomena involved, in computational efficiency, etc., it should be emphasised that the approaches involving transition matrices and dynamic stiffness matrices are equivalent.

REFERENCES

[1] R. BECCU, C.M. WU and B. LUNDBERG 1996 *Journal of Sound and Vibration* **191**(2), 261-272. Reflection and transmission of the energy of transient elastic extensional waves in a bent bar.

[2] I. CARLVIK 1981 *Int. J. Rock Mech. Min. Sci. & Geomech. Abstr.* **10**, 167-172. The generation of bending vibrations in drill rods.

[3] K. F. GRAFF 1975 *Wave motion in elastic solids*. Mineola, New York: Dover Publications, Reprinted edition, 1991.

[4] B. LUNDBERG and A. HENCHOZ 1977 *Experimental Mechanics* **17**(6), 213-218. Analysis of elastic waves from two-point strain measurement.

[5] N. YANAGIHARA 1978 *Bulletin of the Japan Society of Mechanical Engineers* **21**, 1085-1088. New measuring method of impact force.

[6] L. LAGERKVIST AND B. LUNDBERG 1982 *Journal of Sound and Vibration* **80**, 389-399. Mechanical impedance gauge based on measurement of strains on a vibrating rod.

[7] L. LAGERKVIST and K.G. SUNDIN 1982 *Journal of Sound and Vibration* **85**, 473-481. Experimental determination of mechanical impedance through strain measurement on a conical rod.

[8] K.G. SUNDIN 1985 *Journal of Sound and Vibration* **102**, 259-268. Performance test of a mechanical impedance gauge based on strain measurement on a rod.

[9] L.G. KARLSSON, B. LUNDBERG and K.G. SUNDIN 1989 *Int. J. Rock Mech. Min. Sci. & Geomech. Abstr.* **26**, 45-50. Experimental study of a percussive process for rock fragmentation.

[10] B. LUNDBERG, J. CARLSSON and K. G. SUNDIN 1990 *Journal of Sound and Vibration* **137**(3), 483-493. Analysis of elastic waves in non-uniform rods from two-point strain measurement.

[11] J. CARLSSON, K. G. SUNDIN and B. LUNDBERG 1990 *Int. J. Rock Mech. Min. Sci. & Geomech. Abstr.* **27**(6), 553-558. A method for determination of in-hole dynamic force-penetration data from two-point strain measurement on a percussive drill rod.

[12] C. BACON, J. CARLSSON and J. L. LATAILLADE 1991 *Journal de Physique III (Suppl., Colloque C3)* **1**, 395-402. Evaluation of force and particle velocity at the heated end of a rod subjected to impact loading.

[13] C. BACON, J. FÄRM and J. L. LATAILLADE 1994 *Experimental Mechanics* **34**(3), 217-223. Dynamic fracture toughness determined from load-point displacement on a three-point bend specimen using a modified Hopkinson pressure bar.

[14] C. BACON 1998 *Experimental Mechanics* **38**(4), 242-249. An experimental method for considering dispersion and attenuation in a viscoelastic Hopkinson bar.

[15] C. BACON 1999 *International Journal of Impact Engineering* **22**(1), 55-69. Separation of waves propagating in an elastic or viscoelastic Hopkinson pressure bar with three-dimensional effects.

[16] T. SÖDERSTRÖM 1994 *Discrete stochastic systems. Estimation and control.* Cambridge: Prentice Hall International (UK) Limited 1994.

[17] L. HILLSTRÖM, M. MOSSBERG AND B. LUNDBERG 2000 *Journal of Sound and Vibration* 230(3), 689-707. Identification of complex modulus from measured strains on an axially impacted bar using least squares.